INFECTION AND IMMUNITY, Oct. 2003, p. 5845–5854 Vol. 71, No. 10
0019-9567/03/$08.00+0 DOI: 10.1128/IAI.71.10.5845–5854.2003

Widespread Bronchogenic Dissemination Makes DBA/2 Mice More Susceptible than C57BL/6 Mice to Experimental Aerosol Infection with *Mycobacterium tuberculosis*

Pere-Joan Cardona,[1]* Sergi Gordillo,[1] Jorge Díaz,[1] Gustavo Tapia,[2] Isabel Amat,[1] Ángeles Pallarés,[1] Cristina Vilaplana,[1] Aurelio Ariza,[2] and Vicenç Ausina[1]

Unitat de Tuberculosi Experimental, Department of Microbiology,[1] and Department of Pathology,[2] Hospital Universitari "Germans Trias i Pujol" and Universitat Autònoma de Barcelona, Badalona, Catalonia, Spain

Received 4 March 2003/Returned for modification 8 April 2003/Accepted 1 July 2003

We have used the murine model of aerosol-induced experimental tuberculosis to assess the effects of four clinical isolates and a reference strain of *Mycobacterium tuberculosis* on resistant C57BL/6 mice and susceptible DBA/2 mice. Histological studies and detection of 25 cytokines potentially involved in the infection were carried out. DBA/2 mice showed higher concentrations of bacilli in bronchoalveolar lavage fluid and lung tissue. Furthermore, these mice evidenced a larger granulomatous infiltration in the parenchyma due to an increased rate of emigration of infected foamy macrophages from the granulomas to the neighboring pulmonary alveolar spaces. The better control of bacillary concentrations and pulmonary infiltration observed in C57BL/6 mice from week 3 postinfection could result from their higher RANTES, ICAM-1, and gamma interferon (IFN-γ) mRNA levels. On the other hand, the higher MIP-2 and MCP-3 mRNA levels seen in DBA/2 mice would result in stronger lung recruitment of macrophages and neutrophils. Additionally, DBA/2 mice showed increased inducible nitric oxide synthase expression, induced by the larger number of foamy macrophages, at weeks 18 and 22. This increment was a consequence of phagocytosed bacillary debris, was independent of IFN-γ expression, and could exert only a bacteriostatic effect. The results of the study suggest that DBA/2 mice are more susceptible than C57BL/6 mice to *M. tuberculosis* infection due to a higher bronchial dissemination of bacilli inside poorly activated foamy macrophages.

At the beginning of the 21st century, tuberculosis continues to be an important cause of death and a major public health concern. According to World Health Organization estimates, one-third of humankind (2 billion people) is infected with *Mycobacterium tuberculosis*. This extraordinarily high prevalence of the latent infection is one of the main factors contributing to the high incidence of active tuberculosis (more than 8 million new cases per year). Although most infected people never develop active disease, in approximately 10% of cases reactivation of latent infection results in active tuberculosis (49).

Experimental models of murine tuberculosis are of paramount importance for gaining a deeper knowledge of latent infection and the genetic host factors favoring reactivation. Different strains of mice have long been known to have different innate resistances to tuberculous challenge (18, 36). Medina and North first identified susceptibility variations in several inbred mouse strains, showing different survival times after aerosol and intravenous inoculation. These authors related such differences to *bcg* gene (*Nramp1*) and histocompatibility complex haplotype effects (27, 28) and classified six inbred mouse strains as either highly susceptible (CBA, DBA/2, C3H, and 129/SvJ) or highly resistant (BALB/c and C57BL/6).

Many subsequent studies have contributed to a better understanding of the basis for these differences, but the subject still awaits full clarification. Thus, the fact that mycobacteria seem to disseminate earlier from the lungs of resistant mice than from those of susceptible mice has been associated with the stronger response shown by the former (6). It has also been demonstrated that the inability of reactivation-prone mice to recruit lymphocytes to the infection site may underlie their predisposition to chronic-infection control failure and associated bacterial regrowth (46). In the same way, the F_1 progeny of susceptible (I/St) and resistant (A/Sn) parental strains have shown an infection-hyperresistant intermediate phenotype providing a better defense against tuberculosis (25). On the other hand, identification of the genetic basis of susceptibility to tuberculosis has provided deeper insights into immunopathological aspects (20, 24, 30, 33), and the link to the *tbs1* and *tbs2* loci has suggested the existence of a basic genetic network for the control of intracellular parasites (42).

A complex chemokine and cytokine profile is produced during *M. tuberculosis* infection (38). Members of the beta subfamily of chemokines (C-C chemokines), such as macrophage chemotactic protein 1 (MCP-1), macrophage inflammatory protein 1 alpha/beta (MIP-1α/β), and RANTES (regulated upon activation normal T-cell expression sequence), seem to be strongly involved not only in attracting monocytes and lymphocytes to the sites of infection but also in favoring a T helper type 1 (Th1) response (9). Members of the alpha subfamily of chemokines (C-X-C chemokines), such as interferon-inducible protein (IP-10), are usually related to the attraction of neutrophils but also act as potent attractors of monocytes and activated T lymphocytes (22).

* Corresponding author. Mailing address: Unitat de Tuberculosi Experimental, Department of Microbiology, Hospital Universitari "Germans Trias i Pujol," Crta del Canyet s/n, 08916 Badalona, Catalonia, Spain. Phone: 34 93 497 88 94. Fax: 34 93 497 88 95. E-mail: pcardona@ns.hugtip.scs.es.

Generation of specific $CD4^+$ T cells is initiated by the recognition of peptides in the context of major histocompatibility complex class II (MHC II) molecules (12, 23). These $CD4^+$ T cells differentiate into effector cells that are able to produce appropriate levels of cytokines. The early immune response is characterized by the predominance of Th1 cells, which activate infected macrophages through gamma interferon (IFN-γ) production to thwart *M. tuberculosis* growth (11, 17, 34).

It is well known that IFN-γ induces macrophage activation and promotes inducible nitric oxide synthase (iNOS) expression, leading to the production of nitric oxide (NO) and reactive nitrogen intermediates (RNI). It is unclear, however, whether IFN-γ exerts a mycobactericidal (8, 14, 26) or a mycobacteriostatic (13, 16, 39) effect in murine tuberculosis. Be that as it may, IFN-γ augments the acidity of infected phagosomes (45, 48), which seems to be crucial for the enhancement of RNI activity (as is the *M. tuberculosis* strain involved) (39). In contrast, the larger NO amounts produced by murine lung macrophages limit the magnitude of local mucosal T-cell responses by suppressing T-cell activity (44). In this regard, it must be stated that IFN-γ is not solely responsible for the production of NO by macrophages, which can also be elicited by several *M. tuberculosis* cell wall components, such as lipoarabinomannan or the 19-kDa antigen (7).

In the present work, two strains of mice have been infected via aerosol inhalation with four virulent *M. tuberculosis* clinical isolates and strain H37Rv. We provide evidence of susceptibility differences between DBA/2 and C57BL/6 mice, which show dissimilar bacillary concentrations, histopathological findings, and chemokine and cytokine expression profiles (as determined by real-time PCR).

Specifically, susceptibility differences manifested themselves by the early presence in DBA/2 mice of large granulomas with multiple layers of infected foamy macrophages, high CFU counts in bronchoalveolar lavage (BAL) fluid and lung tissue, and low expression of IFN-γ and RANTES in the lung. In contrast, C57BL/6 mice showed smaller and scantier granulomas, moderate CFU counts, and significantly increased IFN-γ and RANTES expression. We have also shown that the higher iNOS expression triggered in DBA/2 mice during the final stages of infection failed to prevent fatal progression. The present study, therefore, suggests that DBA/2 mice are more susceptible to *M. tuberculosis* infection than C57BL/6 mice. Probably this is the consequence of a more widespread bronchogenic dissemination of bacilli transported by insufficiently activated foamy macrophages in DBA/2 mice.

(Part of this research has been presented previously [P. J. Cardona, S. Gordillo, J. Díaz, I. Amat, J. Lonca, and V. Ausina, Abstr. 102nd Gen. Meet. Am. Soc. Microbiol. 2002, abstr. U-61, p. 486, 2002; P. J. Cardona S. Gordillo, J. Díaz, R. Llatjós, A. Ariza, and V. Ausina, Abstr. 5th Int. Conf. Pathog. Mycobacterial Infect. 2002, abstr. P17]).

MATERIALS AND METHODS

Mice. Our study was performed using specific-pathogen-free (*spf*) DBA/2 (*H-2*^{d}) and C57BL/6 (*H-2*^{b}) female mice, 6 to 8 weeks old, which had been obtained from Charles River (Bagneux Cedex, France). Mice were shipped under conditions appropriate for travel, with the corresponding certificate of health and origin. All the animals were kept under controlled conditions in a P3 high-security facility with sterile food and water ad libitum.

Bacteria and infection. The *M. tuberculosis* standard strain NC007416 (H37Rv) and four virulent human clinical isolates were grown in Proskauer Beck medium containing 0.01% Tween 80 to mid-log phase and stored at −70°C in 2-ml aliquots. Mice were placed in the exposure chamber of an airborne infection apparatus (Glas-col Inc., Terre Haute, Ind.). The nebulizer compartment was filled with 7 ml of an *M. tuberculosis* suspension at a concentration previously calculated to provide an uptake of approximately 20 viable bacilli within the lungs. Four mice were used for every time point in every experimental group. The numbers of viable bacteria in homogenates of the left lung and spleen and in BAL fluid at weeks 3, 9, 18, and 22 were monitored by plating serial dilutions on nutrient Middlebrook 7H11 agar (Biomedics s.l., Madrid, Spain) and counting bacterial colony formation after 21 days of incubation at 37°C. Special care was taken not to include hilar lymph nodes at the time of removal of the left lung so as not to artificially increase the CFU count. BAL fluid was obtained by gentle intratracheal injection of 1 ml of phosphate-buffered saline, and lungs were immediately extracted after euthanasia by means of a halothane overdose (Zeneca Farma, Pontevedra, Spain).

Animal health. Mice were weighed once a week. They were supervised every day under a protocol that called for paying attention to weight loss, apparent ill health (bristled hair and wounded skin), and behavior (signs of aggressiveness or isolation). Animals were euthanized by a halothane overdose so as to avoid any suffering. Sentinel animals were used to check *spf* conditions in the facility. Tests for 25 known mouse pathogens were all negative. All experimental proceedings were approved and supervised by the Animal Care Committee of "Germans Trias i Pujol" University Hospital in agreement with the European Union laws for protection of experimental animals.

Histology and morphometry. Histology and morphometry procedures have been described in previous works (32). Briefly, two right lung lobes from each mouse were fixed in buffered formalin and subsequently embedded in paraffin. Every sample was stained with Masson's trichrome stain and hematoxylin-eosin (37). For histometry, 5-μm-thick sections from each specimen were stained with hematoxylin-eosin and photographed at ×50 by using an Eclipse E400 microscope and a Coolpix 990 digital camera (both from Nikon, Tokyo, Japan). Sections of eight lung lobes were studied in each case. By using appropriate software (SigmaScan; SPSS Software, San Rafael, Calif.), the area of each single lesion and the total tissue area were determined on photomicrographs at each time point. Sections were blindly evaluated in order to obtain a more objective measurement.

Immunohistochemistry. Detection of iNOS in lung sections involved procedures described previously (31). Briefly, deparaffinized lung sections were incubated with 0.1 μg of affinity-purified monospecific rabbit immunoglobulin (Ig) against mouse iNOS and NOS type II (BD Transduction Laboratories, Franklin Lakes, N.J.) as the primary antibody. A rabbit polyclonal antibody against the 38-kDa protein of the *M. tuberculosis* cell wall (Novocastra Laboratories, Newcastle upon Tyne, United Kingdom) was also used. In both cases, sections were reacted with biotinylated goat Ig against rabbit Ig as the second reagent, and after a wash, they were incubated with avidin-coupled biotinylated horseradish peroxidase (Vectastain ABC kit; Vector Laboratories, Burlingame, Calif.). Diaminobenzidine was used as the chromogen, according to the supplier's instructions (Vector Laboratories). Photomicrographs were taken with an Eclipse E400 microscope and a Coolpix 990 digital camera. As a negative control, 1% bovine serum albumin–phosphate-buffered saline and an irrelevant antibody from the same species with the same Ig type as the primary antibody were used instead of the primary antibody. As a control of specificity, slides from noninfected mice were included blindly in the process.

RNA extraction and cDNA synthesis. Right middle lobes were homogenized in RNAzol (Cinna/Biotecx, Friendswood, Tex.) by using a glass homogenizer and were snap-frozen to −70°C. Total RNA was extracted by a phenol-chloroform method (10). Total RNA concentrations were determined by spectrophotometry. In addition, a denaturing agarose gel was used to check RNA stability. Total RNA was subjected to a DNase treatment with a DNA-free kit (Ambion, Woodward, Austin, Tex.). Subsequently, 5 μg of RNA was reverse transcribed by using a Superscript RT kit (Gibco BRL, Grand Island, N.Y.) according to the manufacturer's recommendations in order to obtain cDNA.

Quantitative analysis using real time PCR. Quantitative analysis for IFN-γ, tumor necrosis factor alpha (TNF-α), interleukin-1α (IL-1α), IL-2, IL-4, IL-5, IL-6, IL-8r, IL-10, IL-12p40, transforming growth factor beta (TGF-β), iNOS, MIP-1α, MIP-1β, MIP-2, MIP-3α, MIP-3βr, TNF-β (LT-α), MCP-1, MCP-3, intercellular cell adhesion molecule 1 (ICAM-1), RANTES, IP-10, vascular cell adhesion molecule 1 (VCAM-1), and granulocyte-macrophage colony-stimulating factor (GM-CSF) was performed at weeks 0, 3, 9, 18, and 22 postinfection by using a LightCycler system (Roche Biochemicals, Idaho Falls, Idaho). Real-time PCR was carried out in glass capillaries to a final volume of 10 μl in the presence

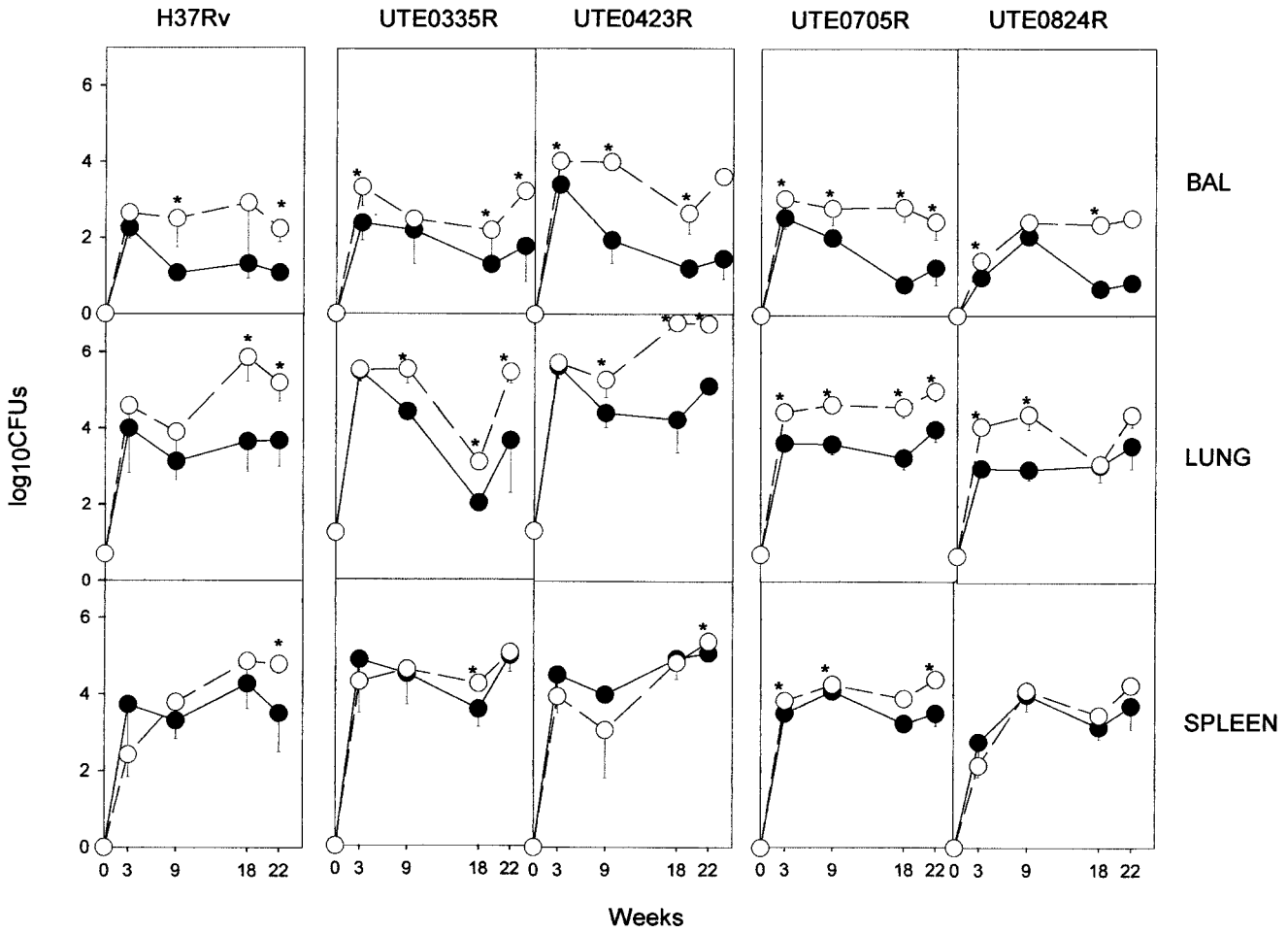

FIG. 1. Evolution of BAL fluid, lung, and spleen bacillary concentrations for each isolate. Data are $\log_{10}$ CFU obtained for each isolate, expressed as means ± standard deviations for four mice. Open and filled symbols, DBA/2 and C57BL/6 mice, respectively. Differences between means were compared using the Student's *t* test. Asterisks indicate significant differences ($P < 0.05$).

of 1 μl of 10× reaction buffer (*Taq* polymerase, deoxynucleoside triphosphates, $MgCl_2$, SYBR Green; Roche Biochemicals) and 1 μl of cDNA (or water as a negative control, which was always included), with $MgCl_2$ added to a final concentration of 2 to 5 mM and primers added to a final concentration of 0.5 μM. For each PCR product, a single peak was obtained by melting curve analysis and only one band of the estimated size was observed on the agarose gel.

Standards for cytokines. PCR was performed in a conventional thermocycler (GeneAmp PCR System 2700; Applied Biosystems, Foster City, Calif.) in order to obtain an unique product for every cytokine with the same primers to be used in the LightCycler. These PCR products were purified in columns of membrane silica (Qiagen purification kit; Qiagen, Valencia, Calif.) and quantified by densitometric comparison to X-174 (Roche Biochemicals) using SigmaScan software (SPSS) on an agarose gel. If only one single band of the predicted size appeared for every cytokine, dilutions were made in order to generate a standard curve plotting Ct values (crossing cycle number) against the known input copy number to enable quantification with the LightCycler software (version 3.5; Roche Biochemicals).

Primer design and normalization to a housekeeping gene. Primers for the cytokines and the housekeeping gene hypoxanthine phosphoribosyltransferase (HPRT) were designed using the LightCycler Probe Design software (Roche Biochemicals). All the primers used are listed on Table 1. HPRT mRNA expression was analyzed for every target sample in order to normalize for efficiencies in cDNA synthesis and RNA input amounts. The ratio to HPRT mRNA expression was obtained for every sample.

Statistical analysis. Sigma Stat (SPSS Software) was used to compare differences among groups by the Student *t* test. Differences were considered significant when P was <0.05.

RESULTS

Evolution of CFU. Evolution of CFU showed the expected tendency (4), although the amounts of BAL fluid and lung tissue bacilli were larger in DBA/2 than in C57BL/6 mice. This higher bacillary concentration was reproducible for all four isolates, but it was not always significant (Fig. 1). In the majority of cases, the increase in bacterial load was not the result of a reactivated chronic infection but the outcome of inferior containment of the early infection, related to higher CFU counts from week 3 postinfection. Concentrations of bacilli in the spleen showed almost no differences between the two mouse strains. The reason why CFU counts in the lungs of animal did not rise any further, including in animals infected with H37Rv, may be that we use a low-dose model of aerosol infection. The fact that we provide an uptake of approximately 20 viable bacilli within the lungs of every animal must be taken into account.

Evolution of granulomatous inflammation. Figures 2 and 3 depict the evolution of pulmonary infiltration by granulomatous lesions. The arithmetical progression shown by this variable over time is the most pronounced genetic difference, es-

TABLE 1. Primer sequences for cytokines and housekeeping gene[a]

Cytokine	Primer	Sequence (5′–3′)	Source or reference
GM-CSF	GM-CSF s	AGATATTCGAGCAGGGT	UTE
	GM-CSF as	AATCCGCATAGGTGGTA	
HPRT	HPRT s	GTTGGATACAGGCCAGACTTTGTTG	3
	HPRT as	GATTCAACTTGCGCTCATCTTAGGC	
ICAM-1	iCAM-1 s	GCCATAAAACTCAAGGGAC	UTE
	iCAM-1 as	GGCTACAAGTGTGCATC	
IFN-γ	IFN-γ s	AGCGGCTGACTGAACTCAGATTGTAG	35
	IFN-γ as	GTCACAGTTTTCAGCTGTATAGGG	
IL-1α	IL-1α s	GTATGCCTACTCGTCGG	UTE
	IL-1α as	CATAGAGGGCAGTCCC	
IL-2	IL-2 s	CCTGAGCAGGATGGAGAATTACA	35
	IL-2 as	TCCAGAACATGCCGCAGAG	
IL-4	IL-4 s	CTAGTTGTCATCCTGCTCTTCTTT	UTE
	IL-4 as	CTTTAGGCTTTCCAGGAAGTCTTT	
IL-5	IL-5 s	CTGGCCTCAAACTGGT	UTE
	IL-5 as	CCCTGATGCAACGAAG	
IL-6	IL-6 s	CCACGGCCTTCCCTAC	UTE
	IL-6 as	AAGTGCATCATCGTTGT	
IL-8r	IL-8r s	GGGTCGTACTGCGTAT	UTE
	IL-8r as	GTCAATGTCATCGCGG	
IL-10	IL-10 s	TTTGAATTCCCTGGGTGAGAA	50
	IL-10 as	ACAGGGGAGAAATCGATGACA	
IL-12p40	IL-12p40 s	AGCACCAGCTTCTTCATCAGG	UTE
	IL-12p40 as	CCTTTCTGGTTACACCCCTCC	
iNOS	iNOS s	CAGCTGGGCTGTACAAACCTT	35
	iNOS as	CATTGGAAGTGAAGCGTTTCG	
IP-10	IP-10 s	GCCGTCATTTTCTGCCTCAT	38
	IP-10 as	GCTTCCCTATGGCCCTCATT	
TNF-β	TNF-β s	CTGTGTATCCGGGACT	UTE
	TNF-β as	CCCTTGAAACAACGGT	
MCP-1	MCP-1 s	AGAGAGCCAGACGGAGGAAG	38
	MCP-1 as	GTCACACTGGTCACTCCTAC	
MCP-3	MCP-3 s	AGGGCATGGAAGTCTG	UTE
	MCP-3 as	TTCCTTAGGCGTGACC	
MIP-1α	MIP-1α s	GTAGCCACATCGAGGG	UTE
	MIP-1α as	TGAGGAACGTGTCCTG	
MIP-1β	MIP-1β s	CCAATGGGCTCTGACCCTCCC	38
	MIP-1β as	CATGTACTCAGTGACCCAGGGC	
MIP-2	MIP-2 s	GCCCCTCCCACCTGCCGGCTGC	38
	MIP-2 as	CTGAACCAGGGGGGCTTCAGGG	
MIP-3α	MIP-3α s	GACTGTTGCCTCTCGT	UTE
	MIP-3α as	TGACTCTTAGGCTGAGGA	
MIP-3β rec	MIP-3β rec s	TGTATGCCTTCATCGGC	UTE
	MIP-3β rec as	GCAGTTTCTTAGGTCCT	
RANTES	RANTES s	GAAGGAACCGCCAAGT	UTE
	RANTES as	AGAGCAAGCGATGACAG	
TGF-β	TGF-β s	GCAACATGTGGAACTCTACCAGAA	50
	TGF-β as	GACGTCAAAAGACAGCCACTCA	
TNF-α	TNF-α s	CATCTTCTCAAAATTCGAGTGACAA	35
	TNF-α as	TGGGAGTAGACAAGGTACAACCC	
VCAM-1	VCAM-1 s	TACACCATCCGCCAGG	UTE
	VCAM-1 as	AGGAGTTCGGGCGAAA	

[a] Forward (s) and reverse (as) primers for HPRT, chemokines, and cytokines are shown. All sequences were obtained from GenBank. Melting temperatures were between 57 and 65°C. Amplicons were kept very short.

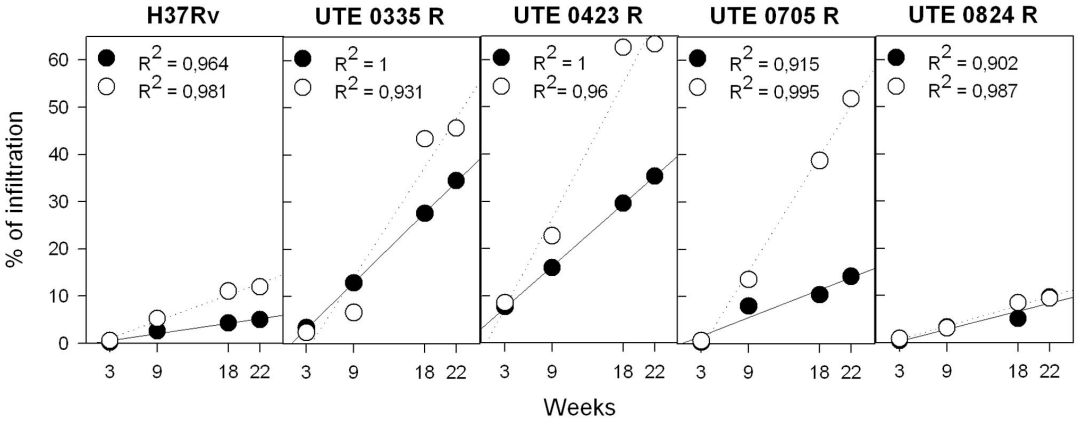

FIG. 2. Evolution of granulomatous infiltration in the lungs. Data are percentages calculated by dividing the granuloma-involved area by the global tissue area and multiplying by 100. Two lung lobes were analyzed for each mouse. Open and filled symbols, DBA/2 and C57BL/6 mice, respectively. Linear regressions were determined by the Pearson product moment correlation coefficient ($P < 0.05$ in all cases).

pecially with regard to DBA/2 mice and isolates UTE 0423R and UTE 0705R, and supports the notion of a progressive process determined by the virulence of the *M. tuberculosis* strain tested from the beginning of the infection. The histological appearance of granulomatous lesions in both mouse strains was essentially as described previously (4). Clustering of neutrophils, macrophages, and lymphocytes, giving rise to primary pregranulomas, was seen during the first weeks postinfection (data not shown). Subsequently, granulomas became better structured, and by week 9, neutrophils, lymphocytes, and macrophages of primary granulomas were surrounded by a thick mantle of lymphocytes (Fig. 4A and E). At the same time, secondary granulomas became visible as compact lesions consisting of abundant lymphocytes that surrounded sparse macrophages (Fig. 4C). Outside this lymphocytic mantle, foamy macrophages were seen to initiate the occupation of alveolar spaces (Fig. 4C). By weeks 18 and 22 postinfection, this alveolar occupation became very noticeable and led to a pronounced size increase and eventual coalescence of granulomas (Fig. 3D and H and 4D, G, and H). In these enlarged granulomas it was possible to distinguish between older layers, rich in disrupted macrophages and cholesterol crystals (Fig. 5B), and newer layers, in which macrophages were well preserved. Additionally, disrupted infected macrophages were accompanied by a progressively denser neutrophilic infiltrate in DBA/2 mice.

Figure 5 depicts the evolution of granuloma-related fibrosis as evidenced by collagen staining with Masson's trichrome technique. Effacement of pulmonary architecture and subtle signs of interstitial fibrosis in association with pregranulomas were already apparent at the beginning of the infection (data not shown). Starting at week 9 postinfection, as granulomas became significantly larger (Fig. 2 and 3), septa surrounding macrophage-filled alveolar spaces showed marked thickening

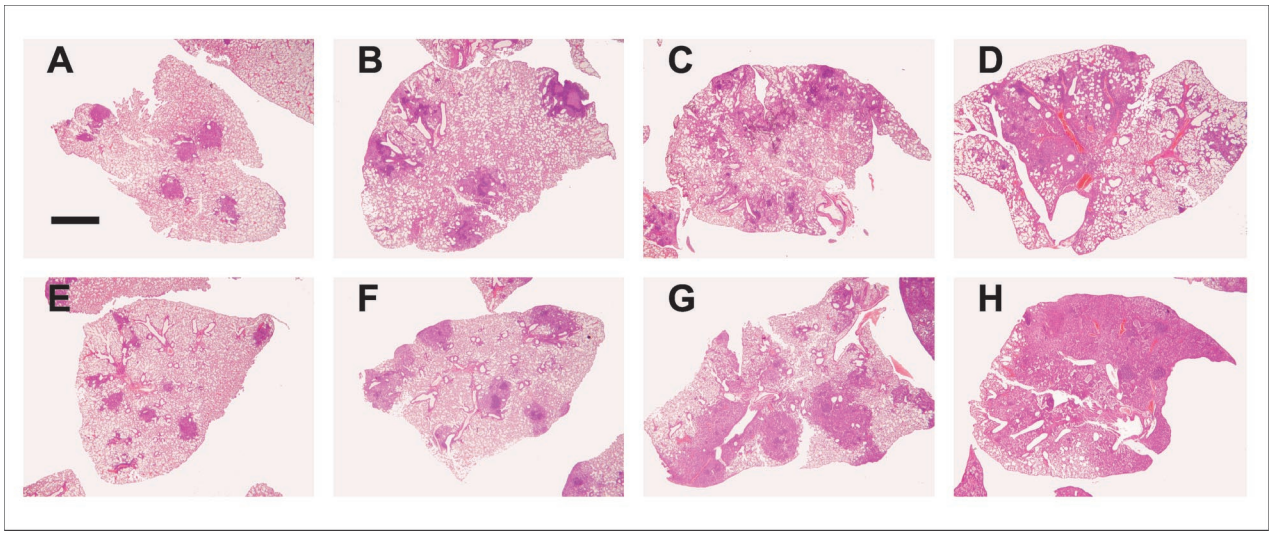

FIG. 3. Evolution of infiltration in C57BL/6 (A through D) and DBA/2 (E through H) mice infected with isolate UTE 0423R at weeks 3 (A and E), 9 (B and F), 18 (C and G), and 22 (D and H) postinfection. Microphotographs were taken with a Nikon stereoscopic microscope SMZ800 (Nikon) at a magnification of ×10. Bar, 500 μm.

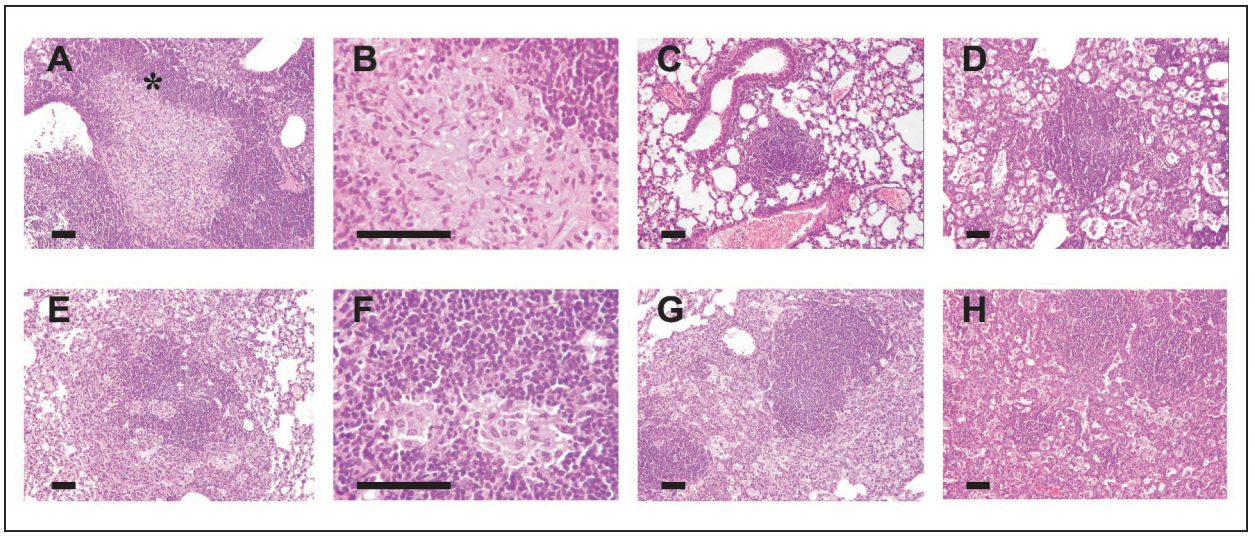

FIG. 4. Evolution of granulomas in C57BL/6 (A through D) and DBA/2 (E through H) mice infected with isolate UTE 0423R at weeks 9 (A through C and E through G) and 22 (D and H) postinfection. (A, B, E, and F) Primary granulomas, with a center of infected macrophages and a mantle of lymphocytes. Panels B and F show intragranulomatous necrosis at a higher power (×400). The asterisk in panel A marks the zone amplified in panel B. (C and G) Secondary and tertiary granulomas, respectively, with a compact center of lymphocytes admixed with scanty infected macrophages. In panel G two secondary granulomas are surrounded by a layer of foamy macrophages that connects them both. (D and H) Tertiary granulomas, with septal thickening of alveoli filled with foamy macrophages. All microphotographs except those in panels B and E were taken at a magnification of ×100. Bars, 100 μm.

secondary to heavy collagen deposition and infiltration by lymphocytes, especially in DBA/2 mice (Fig. 5C and D). Intragranulomatous necrosis is characterized by the accumulation of karyorrhectic debris and fibrillar eosinophilic material accompanied by a strong fibrous reaction within the granuloma. From week 9 postinfection onward, isolates UTE 0335R and UTE 0423R (Fig. 4B) were able to induce intragranulomatous necrosis in C57BL/6 mice but not in DBA/2 mice (Fig. 4F).

Presence of acid-fast bacilli in the lung. At week 3 postinfection, bacilli could be easily visualized within macrophages of pregranulomas. In contrast, at week 9 postinfection, bacilli were hardly discernible within macrophages of primary granulomas (data not shown). The thick lymphocytic mantle surrounding these primary granulomas failed to prevent bacillary dissemination, as evidenced by the fact that single or grouped bacilli were commonly seen within alveolar macrophages outside the lymphocytic mantle (data not shown). Groups of bacilli were more easily identified in DBA/2 mice than in C57BL/6 mice. Bacillus-containing macrophages admixed with abundant neutrophils were also seen in BAL specimens from DBA/2 mice, mostly in the late stages of infection (data not shown).

Production of chemokines and cytokines in the lung. Chemokine and cytokine gene expression in the lung was determined at weeks 0, 3, 9, 18, and 22 postinfection (Fig. 6). No expression of IL-1α, IL-2, IL-4, IL-5, IL-6, MIP-1α, MIP-1β, MCP-1, or VCAM-1 was detected (data not shown). Levels of TNF-α, IL-8r, IL-12p40, MIP-3α, MIP-3βr, TNF-β (LT-α), TGF-β, IP-10, GM-CSF, and IL-10 mRNAs were similar in C57BL/6 and DBA/2 mice (data not shown).

It is noteworthy that IL-1α, IL-6, MIP-1α, MIP-1β, and MCP-1 were not detected, although expression of these chemokines has been reported by other authors (38). We suggest that the absence of expression in the study may be the consequence of a higher specificity due to the technique used to remove DNA and the real-time PCR protocol itself.

C57BL/6 and DBA/2 mice exhibited different induction kinetics for ICAM-1, MCP-3, MIP-2, RANTES, IFN-γ, and iNOS. Expression of the adhesion molecule ICAM-1 was increased in C57BL/6 mice, which clearly facilitates the ability of T lymphocytes to enter the lung. Also meaningful were the higher MCP-3 and MIP-2 mRNA levels detected in DBA/2 mice, since MIP-2 is a potent neutrophil-recruiting chemokine and MCP-3 exerts selective effects on circulating monocytes. As for RANTES, which is associated with a Th1-related immune response in mice, its expression levels were higher in C57BL/6 mice than in DBA/2 mice. Interestingly, in both mouse strains, RANTES expression levels were higher than those of all other chemokines and cytokines. IFN-γ expression levels, also seen to be higher in C57BL/6 mice, peaked at week 3 or 9 postinfection (depending on the *M. tuberculosis* strain) and went down afterwards (3). iNOS mRNA levels increased dramatically in DBA/2 mice at weeks 18 and 22 postinfection, but surprisingly, this surge was neither preceded by increased IFN-γ levels (except for isolate UTE 0824R [data not shown]) nor related to decreased lung bacillary concentrations.

In view of these results, we tried to locate the site of iNOS production by use of immunohistochemistry. Our results did not differ from data obtained by others (31). Thus, iNOS was detected mostly in foamy macrophages (Fig. 7A and C), especially in DBA/2 mice at weeks 18 and 22 postinfection. Similarly, *M. tuberculosis* fragments that were able to induce tissue production of iNOS were mainly located within foamy macrophages (Fig. 7B and D), as described by others (32).

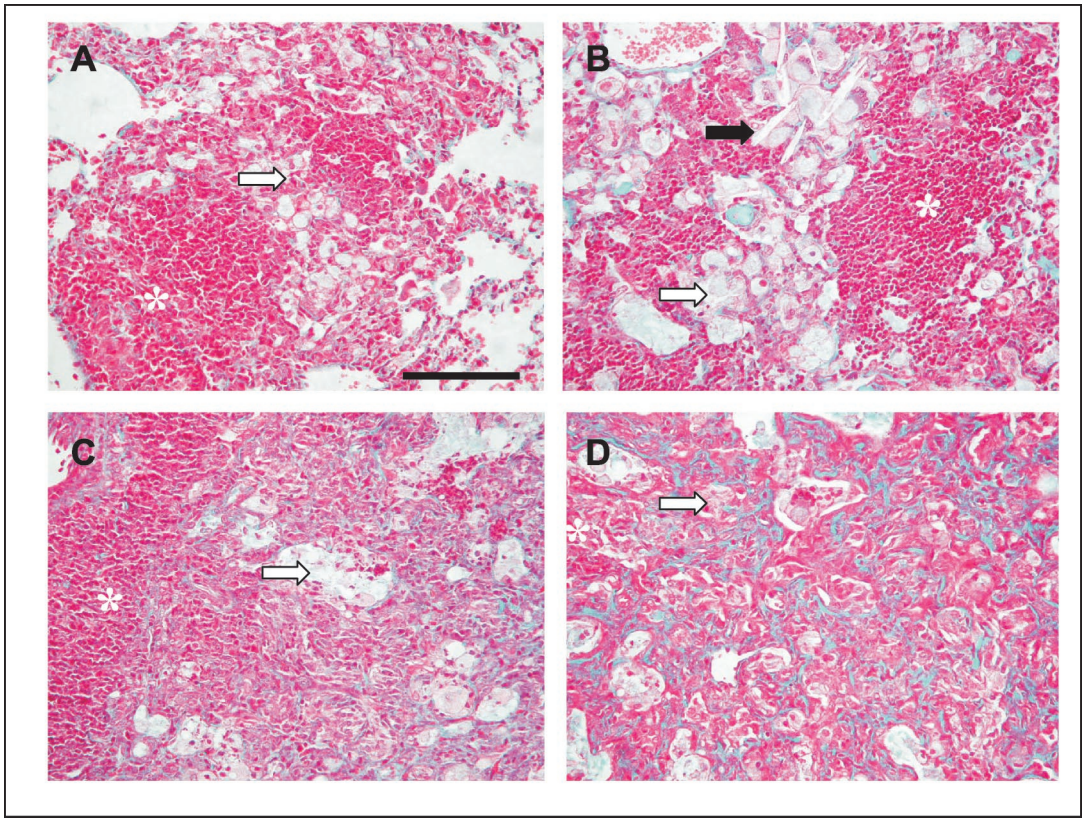

FIG. 5. Fibrosis and inflammation at weeks 9 (A and C) and 18 (B and D) postinfection in C57BL/6 (A and B) and DBA/2 (C and D) mice infected with isolate UTE 0423R. Microphotographs were taken at a magnification of ×200. Bars, 100 μm. Asterisks mark granuloma centers. Black arrow indicates cholesterol crystals; white arrows point to foamy macrophages.

DISCUSSION

As shown by other authors and now confirmed by our study, DBA/2 mice are more susceptible to tuberculous infection than C57BL/6 mice (27, 46). The present work explores the basis of these susceptibility differences. The data obtained support the hypothesis that DBA/2 mice are more susceptible to *M. tuberculosis* aerosol infection because bronchogenic dissemination of bacilli transported by foamy macrophages is more widespread in this strain.

This assertion is well supported by the increased concentrations of bacilli in BAL fluid and lungs, and the accumulation of intra-alveolar macrophages, shown by DBA/2 mice. These higher concentrations were the outcome of less effective containment of the early infection, as CFU counts are higher from week 3 postinfection. In fact, the arithmetic progression of the granulomatous infiltration of the lungs (Fig. 2) lends support to this notion.

Our data expand on previous work that has assigned a paramount role to foamy macrophages in the chronicity of infection in the murine model of tuberculosis. As in other pulmonary infections, foamy macrophages exit granulomas after ingesting debris generated by the inflammatory response (19). Afterwards, macrophages invade alveolar spaces and are propelled by the mucociliary elevator along the bronchial tree to be finally expectorated or swallowed. Previous reports (4, 31, 32) have emphasized that at least some of these foamy macrophages were infected with bacilli. It may be assumed that the survival of bacilli within macrophages is the result of either their insufficient activation by the IFN-γ-induced immune response or new macrophage ingestion of bacilli released from disrupted macrophages. Furthermore, the host immune defenses seem to relax following bacillary destruction associated with the initial response, and afterwards, surviving bacilli adapt to stress conditions by acquiring the so-called latent status. In agreement with this, it has been observed that the mouse immune response is induced by antigens secreted by growing *M. tuberculosis* (12, 34) and that bacilli adopt a different cell wall antigenic composition and a decreased metabolic rate under stress conditions (29).

After the initial steps of chronic infection, far from being enclosed by a fibrous capsule as happens in humans (40), murine granulomas undergo progressive enlargement by occupation of alveolar spaces. Probably the immune response against *M. tuberculosis* in this new scenario is not as efficient as in earlier phases, since disrupted macrophages cannot achieve physical containment of bacilli. Even though the host attracts lymphocytes and deposits collagen in the septa of alveoli filled with foamy macrophages (15), this response is unable to prevent infected cells from disseminating through alveolar spaces.

This disseminating process seems to be more dramatic in DBA/2 mice, in which the weakness of initial IFN-γ induction seems to result in poor activation of infected macrophages. In

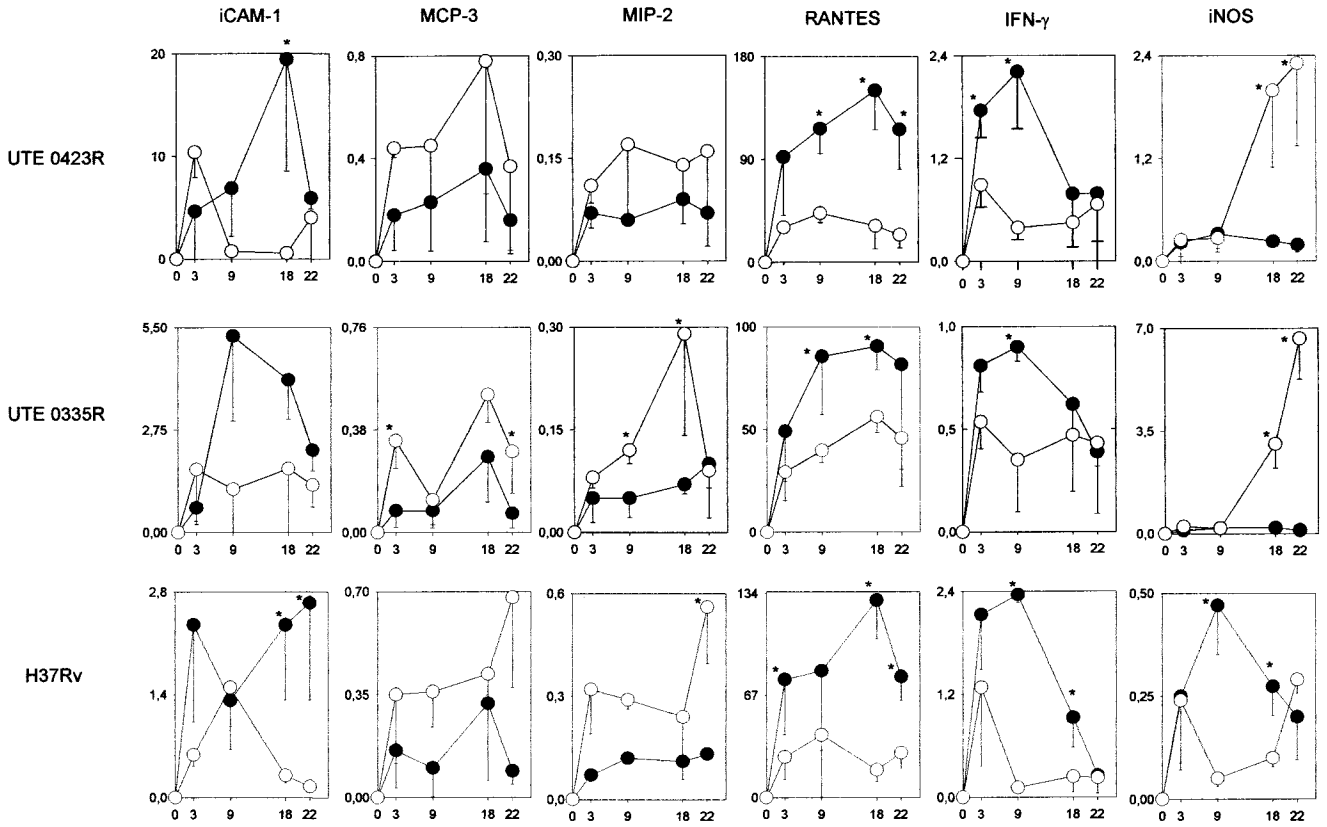

FIG. 6. Evolution of mRNA expression of the chemokines and cytokines that were differently expressed by the two mouse strains, and of iNOS. Results for the most representative *M. tuberculosis* isolates (UTE 0423R, UTE 0335R, and H37Rv) are presented as averages and standard deviations of the ratio of the expression of each particular chemokine or cytokine to that of HPRT in the corresponding sample. Open and filled symbols, DBA/2 and C57BL/6 mice, respectively. The difference between means was determined using Student's *t* test. Asterisks indicate significant differences ($P < 0.05$).

this regard, Baumgart et al. (1) demonstrated that I-A^d MHC class II molecules were expressed on the cell surface in smaller amounts and for shorter periods than I-A^b molecules and that I-A^d molecules induced decreased IFN-γ and increased IL-4 Th2 production compared with activation via I-A^b molecules. These low levels of IFN-γ might also be related to low expression of RANTES and ICAM-1. RANTES is paramount for the building of type 1 granulomas and thus for the attraction of monocytes and the induction of a Th1 response (9, 38). In addition, high expression of ICAM-1 has been related to better localization of lymphocytes to the infection foci, which has been demonstrated by Turner et al. to be crucial for the control of reactivation of the chronic infection in C57BL/6 mice in contrast with CBA/J mice (46). In contrast, higher expression of MCP-3 and MIP-2 mRNAs is probably related to the larger influx of monocytes and neutrophils, respectively, in the lungs (38, 41) and to the increase of the infiltrated area in the lungs and the bronchogenic dissemination of the bacilli.

Our data establish a direct relation between the sizes of lesions and the number of infected, poorly activated macrophages during the early phases of infection. In this scenario, the massive presence of foamy macrophages displaying strong iNOS expression may hamper defenses against bacillary dissemination. This consideration agrees with the finding that alveolar macrophages expressing iNOS are able to transiently suppress T-cell antigen responses through NO-mediated inhibition of tyrosine phosphorylation of T-cell kinases (2, 21, 43, 47).

To explain the enhanced iNOS gene expression taking place at weeks 18 and 22 postinfection in DBA/2 mice, we can invoke possible upregulating effects of IFN-γ, TNF-α, IL-1β, or cell wall components such as LAM and the 19-kDa lipoprotein (7). Since TNF-α and IFN-γ gene expression was not seen to be increased in our work, it can be hypothesized that iNOS levels were upregulated by cell wall components or bacilli ingested by scavenging macrophages. The high iNOS gene expression upregulated by larger amounts of bacillary debris is located mainly on the outer layer of granulomas inside foamy macrophages. We may conclude that this scenario does not mean a reduction in CFU counts in lungs of DBA/2 mice and that the enhanced iNOS expression may exert only a bacteriostatic effect.

It is worth insisting on the importance of using clinical isolates of *M. tuberculosis* instead of the reference strains only. Otherwise, the inflammatory responses of the two mouse strains might have been almost indistinguishable. It should be stressed that C57BL/6 mice, and not DBA/2 mice, developed spontaneous intragranulomatous necrosis after infection with

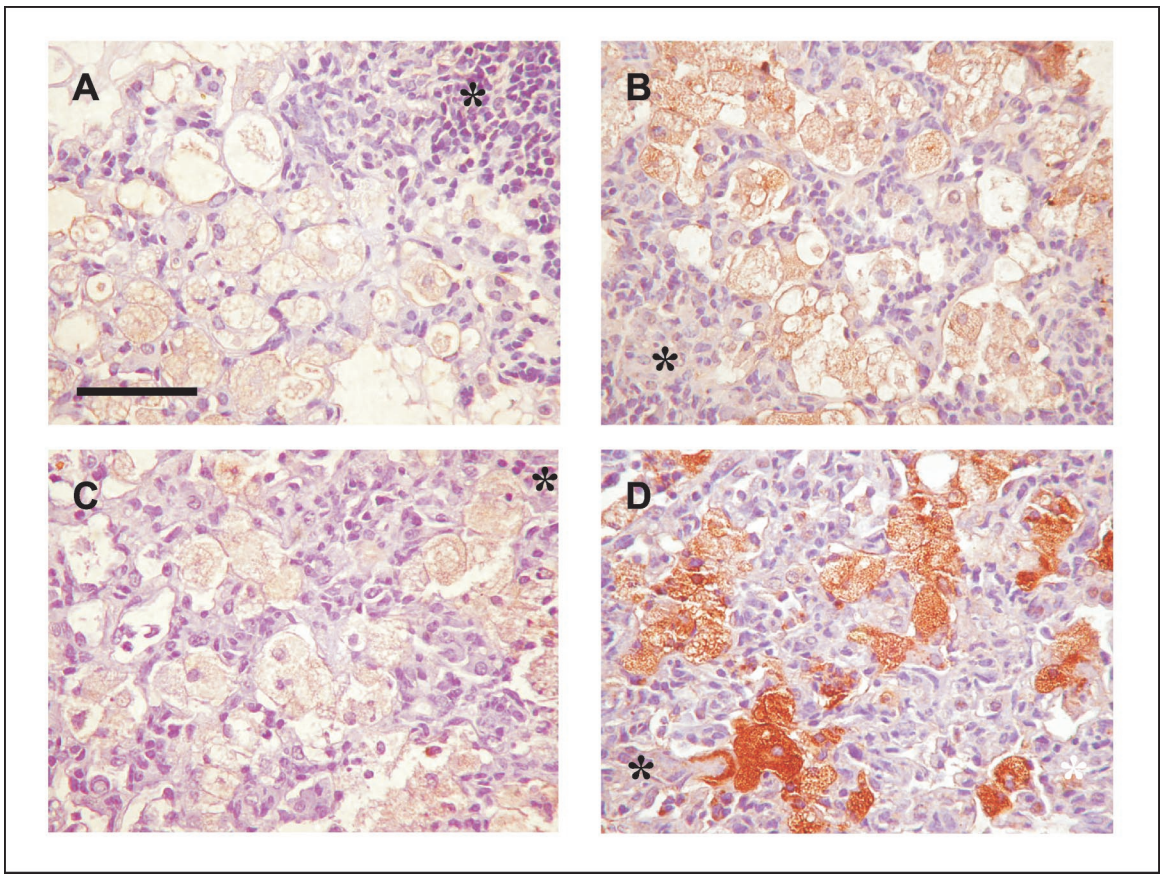

FIG. 7. Immunohistochemistry. Shown is macrophage immunolocalization of iNOS (A and C) and the 38-kDa *M. tuberculosis* cell wall antigen (B and D) in C57BL/6 (A and B) and DBA/2 (C and D) mice infected with isolate UTE 0423R (week 22 postinfection). Microphotographs were taken at a magnification of ×400. Bars, 50 μm. Asterisks mark granuloma centers.

either of two clinical isolates (UTE 0335R and UTE 0423R), a finding very similar to the experimental necrotic changes previously induced by our group (5) and related to an innate host response similar to the Schwartzman reaction. According to those findings, we suggested that endotoxin components of the *M. tuberculosis* cell wall (such as lipoarabinomannan) could be the cause of the intragranulomatous necrosis. More studies must be done in order to elucidate the importance of the composition of the cell wall of those *M. tuberculosis* isolates and to investigate why DBA/2 mice do not develop intragranulomatous necrosis.

Our data are congruent with the possibility of a protective response based on antigen-specific T-cell secretion of IFN-γ leading to macrophage activation and control of the growth of *M. tuberculosis* (11, 34) in C57BL/6 mice. This scenario, supported by large amounts of RANTES (9) and high ICAM expression (46), would promote significant Th1 immune responses, resulting in lower concentrations of bacilli in the lungs. In contrast, DBA/2 mice show a lower Th1 response, displaying higher concentrations of bacilli in the granulomas, which promotes a higher rate of emigration of infected foamy macrophages from initial granuloma structures to surrounding alveolar spaces, progressively increasing the lung pathology.

ACKNOWLEDGMENTS

This work has been funded by grants FIS 99/049-02, 01/0644, and 01/3104 and by grants SEIMC 2000 and 2002 for young researchers.

We thank Marga Ortiz of the Center for Animal Experimentation and the technicians of the Pathology Department, Hospital Universitari Germans Trias i Pujol, for excellent technical support.

REFERENCES

1. **Baumgart, M., V. Moos, D. Schuhbauer, and B. Muller.** 1998. Differential expression of major histocompatibility complex class II genes on murine macrophages associated with T cell cytokine profile and protective/suppressive effects. Proc. Natl. Acad. Sci. USA **95:**6936–6940.
2. **Bilyk, N., and P. G. Holt.** 1995. Cytokine modulation of the immunosuppressive phenotype of pulmonary alveolar macrophage populations. Immunology **86:**231–237.
3. **Cardona, P. J., A. Cooper, M. Luquin, A. Ariza, F. Filipo, I. M. Orme, and V. Ausina.** 1999. The intravenous model of murine tuberculosis is less pathogenic than the aerogenic model owing to a more rapid induction of systemic immunity. Scand. J. Immunol. **49:**362–366.
4. **Cardona, P. J., R. Llatjos, S. Gordillo, J. Díaz, I. Ojanguren, A. Ariza, and V. Ausina.** 2000. Evolution of granulomas in lungs of mice infected aerogenically with *Mycobacterium tuberculosis*. Scand. J. Immunol. **52:**156–163.
5. **Cardona, P. J., R. Llatjos, S. Gordillo, J. Díaz, B. Viñado, A. Ariza, and V. Ausina.** 2001. Towards a 'human-like' model of tuberculosis: intranasal inoculation of LPS induces intragranulomatous lung necrosis in mice infected aerogenically with *Mycobacterium tuberculosis*. Scand. J. Immunol. **53:**65–71.
6. **Chackerian, A. A., J. M. Alt, T. V. Perera, C. C. Dascher, and S. M. Behar.** 2002. Dissemination of *Mycobacterium tuberculosis* is influenced by host factors and precedes the initiation of T-cell immunity. Infect. Immun. **70:**4501–4509.
7. **Chan, E. D., K. R. Morris, J. T. Belisle, P. Hill, L. K. Remigio, P. J. Brennan,**

and D. W. Riches. 2001. Induction of inducible nitric oxide synthase-NO* by lipoarabinomannan of *Mycobacterium tuberculosis* is mediated by MEK1-ERK, MKK7-JNK, and NF-κB signaling pathways. Infect. Immun. **69:**2001–2010.

8. **Chan, J., Y. Xing, R. S. Magliozzo, and B. R. Bloom.** 1992. Killing of virulent *Mycobacterium tuberculosis* by reactive nitrogen intermediates produced by activated murine macrophages. J. Exp. Med. **175:**1111–1122.
9. **Chensue, S. W., K. S. Warmington, E. J. Allenspach, B. Lu, C. Gerard, S. L. Kunkel, and N. W. Lukacs.** 1999. Differential expression and cross-regulatory function of RANTES during mycobacterial (type 1) and schistosomal (type 2) antigen-elicited granulomatous inflammation. J. Immunol. **163:**165–173.
10. **Chomczynski, P., and N. Sacchi.** 1987. Single-step method of RNA isolation by acid guanidinium thiocyanate-phenol-chloroform extraction. Anal. Biochem. **162:**156–159.
11. **Cooper, A. M., D. K. Dalton, T. A. Stewart, J. P. Griffin, D. G. Russell, and I. M. Orme.** 1993. Disseminated tuberculosis in interferon gamma gene-disrupted mice. J. Exp. Med. **178:**2243–2247.
12. **Cooper, A. M., and J. L. Flynn.** 1995. The protective immune response to *Mycobacterium tuberculosis*. Curr. Opin. Immunol. **7:**512–516.
13. **Denis, M.** 1991. Interferon-gamma-treated murine macrophages inhibit growth of tubercle bacilli via the generation of reactive nitrogen intermediates. Cell. Immunol. **132:**150–157.
14. **Denis, M.** 1991. Tumor necrosis factor and granulocyte macrophage-colony stimulating factor stimulate human macrophages to restrict growth of virulent *Mycobacterium avium* and kill avirulent *M. avium*: killing effector mechanism depends on the generation of reactive nitrogen intermediates. J. Leukoc. Biol. **49:**380–387.
15. **Dunn, P. L., and R. J. North.** 1995. Virulence ranking of some *Mycobacterium tuberculosis* and *Mycobacterium bovis* strains according to their ability to multiply in the lungs, induce lung pathology, and cause mortality in mice. Infect. Immun. **63:**3428–3437.
16. **Flesch, I. E., and S. H. Kaufmann.** 1991. Mechanisms involved in mycobacterial growth inhibition by gamma interferon-activated bone marrow macrophages: role of reactive nitrogen intermediates. Infect. Immun. **59:**3213–3218.
17. **Flynn, J. L., J. Chan, K. J. Triebold, D. K. Dalton, T. A. Stewart, and B. R. Bloom.** 1993. An essential role for interferon gamma in resistance to *Mycobacterium tuberculosis* infection. J. Exp. Med. **178:**2249–2254.
18. **Forget, A., E. Skamene, P. Gros, A. C. Miailhe, and R. Turcotte.** 1981. Differences in response among inbred mouse strains to infection with small doses of *Mycobacterium bovis* BCG. Infect. Immun. **32:**42–47.
19. **Green, G. M.** 1973. Alveolobronchiolar transport mechanisms. Arch. Intern. Med. **131:**109–114.
20. **Gros, P., E. Skamene, and A. Forget.** 1983. Cellular mechanisms of genetically controlled host resistance to *Mycobacterium bovis* (BCG). J. Immunol. **131:**1966–1972.
21. **Holt, P. G.** 1993. Regulation of antigen-presenting cell function(s) in lung and airway tissues. Eur. Respir. J. **6:**120–129.
22. **Kaplan, G., A. D. Luster, G. Hancock, and Z. A. Cohn.** 1987. The expression of a gamma interferon-induced protein (IP-10) in delayed immune responses in human skin. J. Exp. Med. **166:**1098–1108.
23. **Kaufmann, S. H.** 1995. Immunity to intracellular microbial pathogens. Immunol. Today **16:**338–342.
24. **Lengeling, A., K. Pfeffer, and R. Balling.** 2001. The battle of two genomes: genetics of bacterial host/pathogen interactions in mice. Mamm. Genome **12:**261–271.
25. **Lyadova, I. V., E. B. Eruslanov, S. V. Khaidukov, V. V. Yeremeev, K. B. Majorov, A. V. Pichugin, B. V. Nikonenko, T. K. Kondratieva, and A. S. Apt.** 2000. Comparative analysis of T lymphocytes recovered from the lungs of mice genetically susceptible, resistant, and hyperresistant to *Mycobacterium tuberculosis*-triggered disease. J. Immunol. **165:**5921–5931.
26. **MacMicking, J. D., R. J. North, R. LaCourse, J. S. Mudgett, S. K. Shah, and C. F. Nathan.** 1997. Identification of nitric oxide synthase as a protective locus against tuberculosis. Proc. Natl. Acad. Sci. USA **94:**5243–5248.
27. **Medina, E., and R. J. North.** 1998. Resistance ranking of some common inbred mouse strains to *Mycobacterium tuberculosis* and relationship to major histocompatibility complex haplotype and Nramp1 genotype. Immunology **93:**270–274.
28. **Medina, E., B. J. Rogerson, and R. J. North.** 1996. The Nramp1 antimicrobial resistance gene segregates independently of resistance to virulent *Mycobacterium tuberculosis*. Immunology **88:**479–481.
29. **Michele, T. M., C. Ko, and W. R. Bishai.** 1999. Exposure to antibiotics induces expression of the *Mycobacterium tuberculosis sigF* gene: implications for chemotherapy against mycobacterial persistors. Antimicrob. Agents Chemother. **43:**218–225.
30. **Mitsos, L. M., L. R. Cardon, A. Fortin, L. Ryan, R. LaCourse, R. J. North, and P. Gros.** 2000. Genetic control of susceptibility to infection with *Mycobacterium tuberculosis* in mice. Genes Immun. **1:**467–477.
31. **Mogues, T., M. E. Goodrich, L. Ryan, R. LaCourse, and R. J. North.** 2001. The relative importance of T cell subsets in immunity and immunopathology of airborne *Mycobacterium tuberculosis* infection in mice. J. Exp. Med. **193:**271–280.
32. **Mustafa, T., S. Phyu, R. Nilsen, R. Jonsson, and G. Bjune.** 1999. A mouse model for slowly progressive primary tuberculosis. Scand. J. Immunol. **50:**127–136.
33. **Nikonenko, B. V., M. M. Averbakh, Jr., C. Lavebratt, E. Schurr, and A. S. Apt.** 2000. Comparative analysis of mycobacterial infections in susceptible I/St and resistant A/Sn inbred mice. Tuber. Lung Dis. **80:**15–25.
34. **Orme, I. M., P. Andersen, and W. H. Boom.** 1993. T cell response to *Mycobacterium tuberculosis*. J. Infect. Dis. **167:**1481–1497.
35. **Overbergh, L., D. Valckx, M. Waer, and C. Mathieu.** 1999. Quantification of murine cytokine mRNAs using real time quantitative reverse transcriptase PCR. Cytokine **11:**305–312.
36. **Pierce, C., R. Dubos, and G. Middlebrook.** 1947. Infection of mice with mammalian tubercle bacilli grown in Tween-albumin liquid medium. J. Exp. Med. **86:**159–174.
37. **Prophet, E. B., B. Mills, J. B. Arrington, and L. H. Sobin (ed.).** 1992. AFIP laboratory methods in histotechnology. American Registry of Pathology, Washington, D.C.
38. **Rhoades, E. R., A. M. Cooper, and I. M. Orme.** 1995. Chemokine response in mice infected with *Mycobacterium tuberculosis*. Infect. Immun. **63:**3871–3877.
39. **Rhoades, E. R., and I. M. Orme.** 1997. Susceptibility of a panel of virulent strains of *Mycobacterium tuberculosis* to reactive nitrogen intermediates. Infect. Immun. **65:**1189–1195.
40. **Ridley, D. S., and M. J. Ridley.** 1987. Rationale for the histological spectrum of tuberculosis. A basis for classification. Pathology **19:**186–192.
41. **Rollins, B. J.** 2001. MCP-1, MCP-2, MCP-3, MCP-4 and MCP-5, p. 1145–1160. *In* J. J. Oppenheim and M. Feldmann (ed.), Cytokine reference, vol 1. Academic Press, San Diego, Calif.
42. **Sanchez, F., T. V. Radaeva, B. V. Nikonenko, A. S. Persson, S. Sengul, M. Schalling, E. Schurr, A. S. Apt, and C. Lavebratt.** 2003. Multigenic control of disease severity after virulent *Mycobacterium tuberculosis* infection in mice. Infect. Immun. **71:**126–131.
43. **Strickland, D., U. R. Kees, and P. G. Holt.** 1996. Regulation of T-cell activation in the lung: alveolar macrophages induce reversible T-cell anergy in vitro associated with inhibition of interleukin-2 receptor signal transduction. Immunology **87:**250–258.
44. **Stumbles, P. A., A. S. McWilliam, and P. G. Holt.** 1999. Dendritic cells and mucosal macrophages, p. 397–412. *In* P. L. Ogra, J. Mestecky, M. E. Lamm, W. Strober, J. Bienenstock, and J. R. McGhee (ed.), Mucosal immunology. Academic Press, San Diego, Calif.
45. **Tsang, A. W., K. Oestergaard, J. T. Myers, and J. A. Swanson.** 2000. Altered membrane trafficking in activated bone marrow-derived macrophages. J. Leukoc. Biol. **68:**487–494.
46. **Turner, J., M. Gonzalez-Juarrero, B. M. Saunders, J. V. Brooks, P. Marietta, D. L. Ellis, A. A. Frank, A. M. Cooper, and I. M. Orme.** 2001. Immunological basis for reactivation of tuberculosis in mice. Infect. Immun. **69:**3264–3270.
47. **Upham, J. W., D. H. Strickland, N. Bilyk, B. W. Robinson, and P. G. Holt.** 1995. Alveolar macrophages from humans and rodents selectively inhibit T-cell proliferation but permit T-cell activation and cytokine secretion. Immunology **84:**142–147.
48. **Via, L. E., R. A. Fratti, M. McFalone, E. Pagan-Ramos, D. Deretic, and V. Deretic.** 1998. Effects of cytokines on mycobacterial phagosome maturation. J. Cell Sci. **111:**897–905.
49. **World Health Organization.** 2001. Global tuberculosis control. WHO Report 2001. WHO/CDS/TB/2001.287. World Health Organization, Geneva, Switzerland.
50. **Xia, D., A. Sanders, M. Shah, A. Bickerstaff, and C. Orosz.** 2001. Real-time polymerase chain reaction analysis reveals an evolution of cytokine mRNA production in allograft acceptor mice. Transplantation **72:**907–914.

Editor: S. H. E. Kaufmann